JOURNAL OF APPLIED ELECTROCHEMISTRY 17 (1987) 196–204

Kinetics of anodic oxide film growth on indium in alkaline solution

S. J. DUNCAN, G. T. BURSTEIN

Department of Metallurgy and Materials Science, University of Cambridge, Pembroke Street, Cambridge CB2 3QZ, UK

Received 5 February 1986; revised 22 March 1986

Data are presented which describe the kinetics of repassivation of freshly generated indium surfaces of pH 14. The process is controlled by ion conduction through the growing oxide film under high electric field. The associated kinetic parameters are tabulated. At high potentials an excess anodic charge is observed; it is attributed to conversion of some of the barrier film into an non-barrier layer. Some kinetic data associated with this process are presented.

1. Introduction

Despite the interest in indium as a battery anode for alkaline cells, little is known of the kinetics of oxide film growth. Early work [1, 2] showed that the metal oxidized to produce a film of In_2O_3 or $In(OH)_3$ and that current densities of more than 1 mA cm^{-2} can be drawn through this oxide. Boswell [2] reported that the electrode may be stored in alkaline solution without appreciable deterioration, although it will function usefully when current is drawn. Such stability is also described by Pourbaix [3] for indium in solutions of pH 13–15. The current drawn from the anode could be increased greatly by alloying indium with lead or bismuth [2].

Structural analysis of the oxide film formed has been performed by electron diffraction [4, 5]. The work pertains to oxide films grown on 1 at % indium amalgams, however, and it is very unlikely that such a dilute alloy would give a film of characteristics similar to that formed on pure indium. Similarly, the kinetics of film growth and reduction described for the amalgams [4, 5] are also likely to be different.

Measurements using galvanostatic pulse experiments [6, 7] were confined to low overpotentials with respect to the indium–indium oxide equilibrium (up to $\eta \sim 15$ mV; exceptionally up to $\eta \sim 70$ mV) and the exchange current density was determined using the polarization resistance. Such galvanostatic pulse data for indium are ambiguous in that the equilibrium between indium and In_2O_3 lies some 170 to 190 mV below that between H_2O and H_2, and thus such surfaces cannot be free both of oxide films and of reduced hydrogen simultaneously. The ambiguity can be resolved by generating a fresh metal surface *in situ*.

Work on the indium electrode has been reviewed by Piercy and Hampson [8].

2. Experimental details

The kinetics of anodic oxide film growth on indium (99.98% Johnson-Matthey) were examined using the scratched rotating disc electrode. This technique has been described in detail elsewhere [9] and consists of generating a scratch for a short period of time (3–4 ms for the present results) on the surface of a rotating disc electrode held under potential control. The scratch, which is generated by a diamond stylus, measures ~ 1.5 mm long $\times$ 78 μm wide $\times$ 16 μm maximum depth on indium. The consequent current transient is recorded using a bank of transient recorders (Datalab) and a digital voltmeter (Solartron) acting as an analogue-to-digital convertor interfaced with a microcomputer. In this way current transients were collected over some 4 to 5 orders of magnitude in current and time and stored on disc. An

0021–891X/87 $03.00 + .12

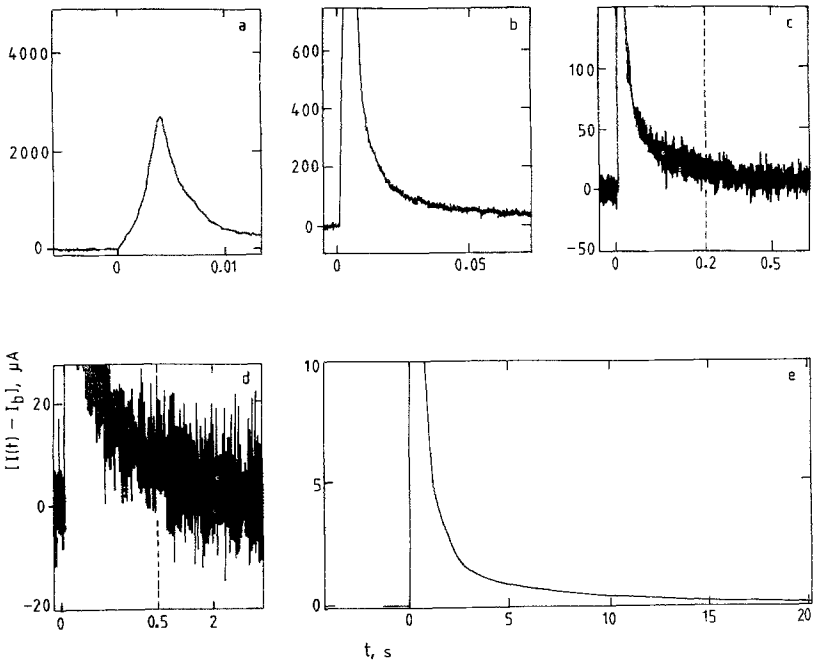

Fig. 1. Anodic current transient arising from reactions of a scratch generated on indium in 1.0 M KOH at $E = -655$ mV (versus SHE). The five sections (a–e) describe the same transient measured over different sensitivity and time scales.

example of a current transient on indium is shown in Fig. 1, in which all five sections covering a large range of current and time are displayed. In order for the current transient to be readily interpretable, two criteria should be met. The first is that the scratch penetrates completely any preformed oxide film existing on the metal surface so that the measured surface area (see below) represents that associated with the freshly generated metal surface; this was true for the present work. The second is that the base current, I_b, flowing from the electrode before scratching has reached a steady state. This was achieved for indium in alkaline solution by allowing I_b to stabilize for periods of between 20 and 90 min, the exact time depending on the applied potential.

The electrolyte used was 1.0 M KOH, pH 14, made from analytical grade reagent and doubly distilled water; this solution was thoroughly purged with purified nitrogen before and during measurements. Experiments were performed at ambient temperature (19 ± 2° C) with the electrode rotating at ~ 100 Hz.

3. Results

Current transients are quantified as follows. We define the maximum *observed* bare surface current density as

$$i_s = \frac{1}{2\pi r\omega y}\left(\frac{dI}{dt}\right) \qquad (1)$$

where dI is the increase in current in time, dt, during scratching, y is the scratch width, r is its distance from the centre of rotation and ω is the rotation rate. The current density is thus defined by the increase in observed current due to the increased scratch area as the scratch is being generated. The decay of current on the scratch with time after the scratch is complete is given by

$$i(t) = \frac{1}{2\pi r\omega y t_c}[I(t) - I_b] \qquad (2)$$

where $I(t)$ is the current flowing from the whole electrode including the scratch at time t after scratching, and t_c is the stylus contact time. The charge density $q(t)$ that has flowed from the

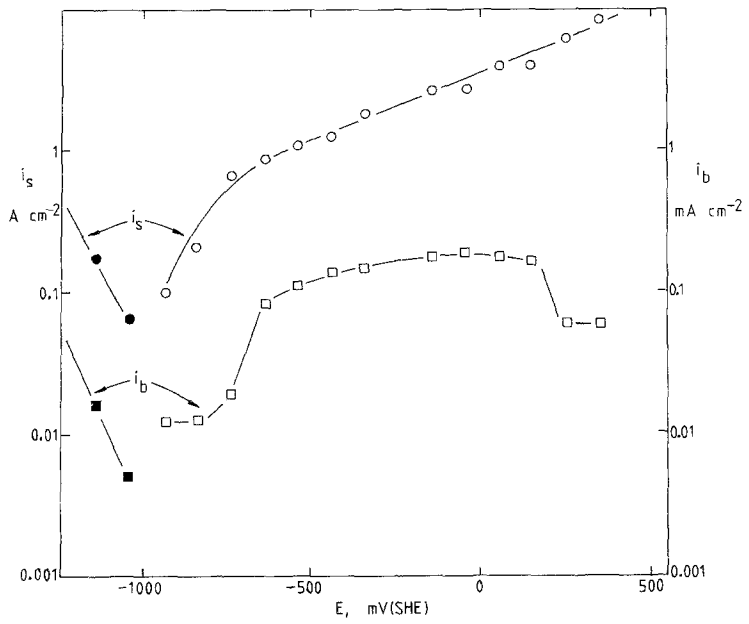

Fig. 2. Steady-state (squares) and maximum observed bare surface (circles) polarization curves for indium in 1.0 M KOH. White symbols represent anodic; black symbols represent cathodic. Note that the ordinate for i_s is marked in A cm^{-2}; that for i_b is marked in mA cm^{-2}.

scratch at t is given by

$$q(t) = \frac{1}{2\pi r\omega y t_c}\int_0^t [I(t) - I_b]\,dt \qquad (3)$$

In the above equations the scratch surface area is given as $2\pi r\omega y t_c$ and the scratch depth is thereby ignored.

The maximum observed bare surface current density, i_s, is plotted as a polarization curve in Fig. 2. To show the enormous acceleration in anodic reaction rate caused by the scratch the values of the steady-state base current density, i_b, are also shown. The anodic values of i_s range between ~ 0.1 and $\sim 10\,\mathrm{A\,cm^{-2}}$, representing an acceleration of some 4 orders of magnitude over i_b. The anodic value of i_s shows a continuous increase with increase in E, but the rate of increase of log i_s with E falls as E rises.

The transients were recorded at 100 mV intervals and the lowest potential at which accelerated anodic behaviour on the scratch was observed was -955 mV (versus SHE). At -1055 mV (versus SHE) the net scratch current was cathodic and at this potential the base current was also cathodic. The bare surface mixed potential (defined by zero net current on the scratch) and the steady-state mixed potential, therefore, lie between these two values of the electrode potential. The cathodic transients will not be discussed in this paper.

Decay of current density on the scratch with time was documented over several orders of magnitude. Some current decay plots are shown in Fig. 3. The scratch current commences decay immediately on cessation of the scratching process. The initial decay occurs with $\partial \log i(t)/\partial \log t \simeq -1$. Inspection of the graphs over a long time span, however, shows that the plots bend towards longer times at lower current densities. They therefore show gentle curvature, but it requires measurement over some 4 to 5 orders of magnitude in time for this to be observed clearly. It should be noted that plotting of log $i(t)$ versus log t requires definition of the position $t = 0$. Because of the finite time required to form the scratch (t_c) this position is uncertain, the earliest formed parts of the scratch being the oldest. We have used the point of stylus contact as $t = 0$ in order to plot Fig. 3. An uncertainty is consequently introduced into the very early rate of current decay which has the effect of steepening the graph in the early time region. This uncertainty becomes negligible for $t > \sim 10$ ms.

The decay in scratch current density as a function of the total charge density passed on the

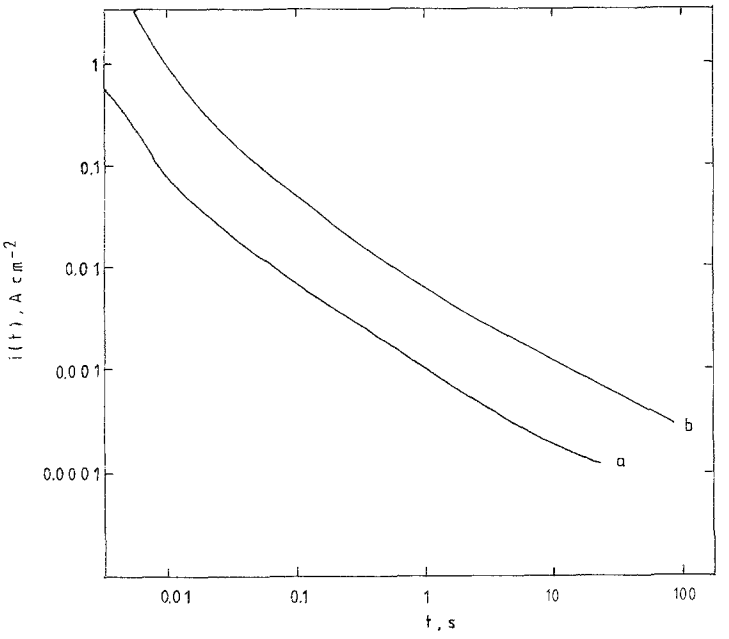

Fig. 3. Decay of current density with time for repassivation of scratched indium in 1.0 M KOH at potentials of (a) −655 mV (versus SHE) and (b) +45 mV (versus SHE).

scratch, $q(t)$, is shown in Fig. 4 for two different potentials. The form of the graph, log $i(t)$ versus $q(t)^{-1}$, is discussed below. At high $i(t)$ these graphs are curved but show a range of linearity in which log $i(t) \propto q(t)^{-1}$ over some two orders of magnitude in current density. This behaviour was characteristic of the anodic scratch current density for indium at pH 14 at all potentials up to +145 mV (versus SHE). Furthermore, the graphs lie at higher charge densities for higher electrode potentials. The lines shown in Fig. 4 span the approximate range $3 < q(t) < 12\,\mathrm{mC\,cm^{-2}}$, and this provides the region in which the above relationship is valid. For $E > +145$ mV (versus SHE) the graphs lie at higher charge densities and the range extends to some $100\,\mathrm{mC\,cm^{-2}}$.

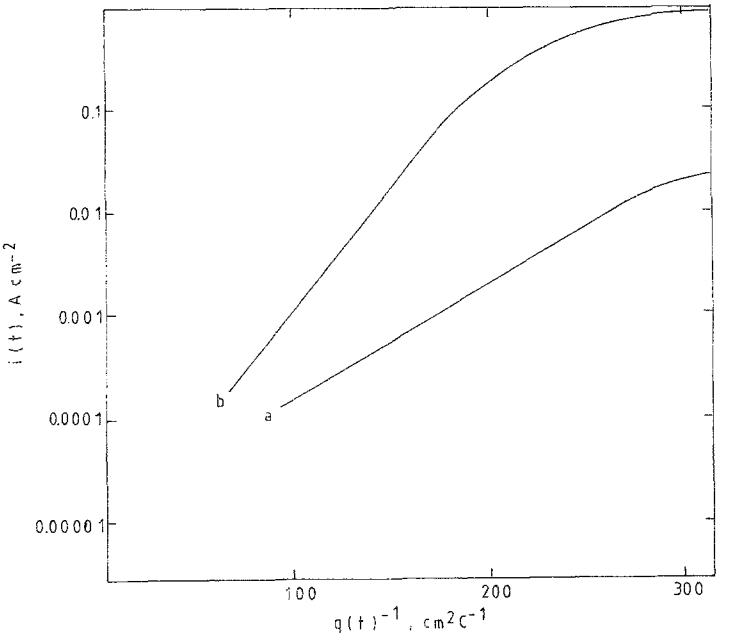

Fig. 4. Repassivation of indium in 1.0 M KOH at a function of the charge density passed at potentials of (a) −655 mV (versus SHE) and (b) −155 mV (versus SHE).

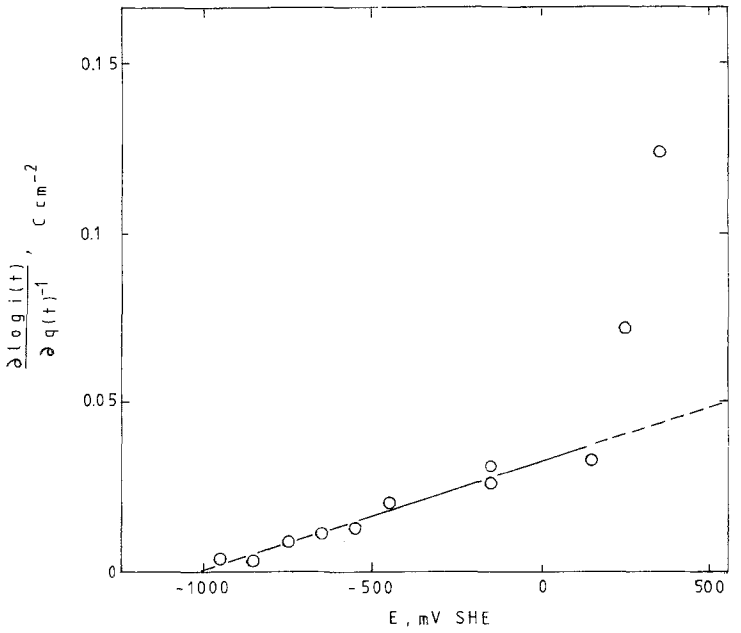

Fig. 5. High-field current decay gradient (Equation 7) as a function of potential for indium respassivating in 1.0 M KOH.

4. Discussion

The fact that the current decays immediately the stylus leaves the metal surface implies that repassivation also commences immediately. This observation is consistent with the behaviour of many freshly generated metal surfaces [9–12], but not all [13]. The rate of current decay can thus be modelled in terms of oxide film growth and we now show that the kinetics are fully consistent with this phenomenon.

The kinetics of film growth controlled by rate limitation of ion conduction under high electric field are given by [14]:

$$i(t) = \bar{A} \exp\left[\frac{BV(t)}{x(t)}\right] \quad (4)$$

where $\bar{A}$ and B are constants and $V(t)$ is the voltage drop across a film of thickness $x(t)$, both at time t. We make the following assumptions in line with previous work [10]. First, all the anodic charge density evolved goes towards formation of the barrier film and no other process is involved. (It is shown below that for $E > +145$ mV, versus SHE, extra anodic charge density is indeed evolved, and this is modelled in terms of formation of a *non-barrier* film.) Second, the voltage drop, $V(t)$, across the film is constant with time (for constant applied potential) and at any time it provides a uniform electric field through the film. Thus

$$x(t) = \frac{Mq(t)}{zF\varrho} \quad (5)$$

where M is the molecular weight of the film, ϱ is its density and z is the charge number on the current carrying ion, and $V(t)$ is replaced by $E - E_g$ where E is the applied electrode potential and E_g is the minimum potential for which Equation 4 is followed. Rearranging Equation 5 gives

$$\log i(t) = \log \bar{A} + \frac{BzF\varrho(E - E_g)}{2.3Mq(t)} \quad (6)$$

where $\log i(t) \propto q(t)^{-1}$.

Fig. 4 shows that Equation 6 is obeyed by the experimental data for $i(t) \lesssim 1\,\mathrm{A\,cm^{-2}}$ and for $E < \sim +145$ mV (versus SHE). Some 2 to 3 orders of magnitude in current density are covered in this way. Differentiation of Equation 6 gives

$$\frac{\partial \log i(t)}{\partial q(t)^{-1}} = \frac{BzF\varrho}{2.3M}(E - E_g) \quad (7)$$

A plot of this gradient against E should thus be linear, of slope $BzF\varrho/2.3M$ and intercept E_g. The graph is shown in Fig. 5 and is linear for $E < +145$ mV (versus SHE). The above

Table 1. Kinetic parameters associated with the repassivation of indium at pH 14 according to Equation 6

E (mV versus SHE)	$\frac{\partial \log i(t)}{\partial q(t)^{-1}}$ *(C cm^{-2})*	*log $\bar{A}$ (A cm^{-2})*
−955	0.0044	−4.7
−855	0.0030	−5.1
−755	0.0086	−4.8
−655	0.011	−4.9
−555	0.013	−4.8
−455	0.020	−5.2
−155	0.026	−4.5
−155	0.031	−5.0
45	0.089	−4.5
145	0.032	−5.3
245	0.072	−4.9
345	0.12	−5.6
Mean		−4.94 ± 0.31

assumptions are therefore deemed to be correct although small amounts of excess charge such as could be involved in dissolution processes from the freshly generated metal surface may not affect Figs 4 and 5 significantly. Using Figs 4 and 5 it is possible to calculate the values of $\bar{A}$ and B above, provided values of z, ϱ and M are assumed. For this purpose we put $z = 6$, $\varrho = 7.179\,\mathrm{g\,cm^{-3}}$ and $M = 277.64\,\mathrm{g\,mol^{-1}}$ for In_2O_3 [15]. This gives the values of $\bar{A}$ and B shown in Table 1. The mean values of these, $\log \bar{A}$, $(\mathrm{A\,cm^{-2}}) = -4.94 \pm 0.31$ and $B = (4.8 \pm 0.3) \times 10^{-6}\,\mathrm{cm\,V^{-1}}$, are consistent with those obtained for a number of other oxide growth systems [10, 11, 16]. These values can be interpreted as [17]:

$$B = \frac{bez}{kT} \tag{8}$$

and

$$A = zevn \exp\left(\frac{-\phi}{kT}\right) \tag{9}$$

where e is the electron charge, k is the Boltzmann constant, n is the number of mobile ions available of vibrational frequency, v, and ϕ and b are respectively the height and half-width of the energy barrier through which these ions pass. Using the values $n = 10^{15}\,\mathrm{cm^{-2}}$, $v = 6 \times 10^{12}\,\mathrm{Hz}$ and $T = 292\,\mathrm{K}$ we calculate the mean values of $b = 0.40\,\mathrm{nm}$ and $\phi = 0.13\,\mathrm{aJ}$. The values are reasonable [17]. In particular, b would be estimated to be about half a lattice spacing in In_2O_3 [18]; the full lattice spacing is $\sim 1\,\mathrm{nm}$ in agreement with b above.

The value of $E_g = -1017\,\mathrm{mV}$ (versus SHE) should be compared with the potential for equilibrium, E_0, between indium and its oxide at pH 14. Pourbaix [3] has calculated E_0 to be $-1017\,\mathrm{mV}$ (versus SHE) for anhydrous In_2O_3 and $-999\,\mathrm{mV}$ (versus SHE) for hydrated In_2O_3. The measured value of E_g cannot distinguish the two values of E_0, but is clearly in excellent agreement with both, where $E_g = E_0$.

In addition, the metal shows no evidence of accelerated anodic behaviour on the scratch at potentials lower than this. The bare surface mixed potential shown in Fig. 2 is the same as the steady-state mixed potential (also from Fig. 2), and both are also consistent with E_g and E_0. All these four potentials are therefore equal and the metal shows no evidence of oxidation at an underpotential. Some metals do, in fact, show growth of the first monolayer of oxide at $E < E_0$ [19, 20].

The high current regions of Fig. 4 do not follow Equation 6. The reasons for this lie in the significantly high ohmic potential drop in this region and in the fact that anodic film growth is probably not uniform over the scratch in the early stages. Comparison of Figs 3 and 4 shows that obedience to Equation 3 commences at $t \simeq 10$–$15\,\mathrm{ms}$; for times earlier than this the earliest formed parts of the scratch have repassivated significantly further than the later formed parts, owing to the relatively long contact time, t_c, of 3 ms.

The scratch-current decay relationship for $E \geqslant +145\,\mathrm{mV}$ (versus SHE) deviates from the behaviour described above. We see from Fig. 4 that such graphs lie at higher charge densities than expected from Equation 6, and this is reflected also in Fig. 5 which shows deviation from Equation 7 at these high potentials. It is important to note that the excess anodic charge associated with these transients is not due to oxygen evolution on the bare metal surface; this process has an equilibrium potential at pH 14 and 1 atm O_2 of $+402\,\mathrm{mV}$ (versus SHE) which is too high for the observed transients. The data are modelled as follows. We assume barrier film

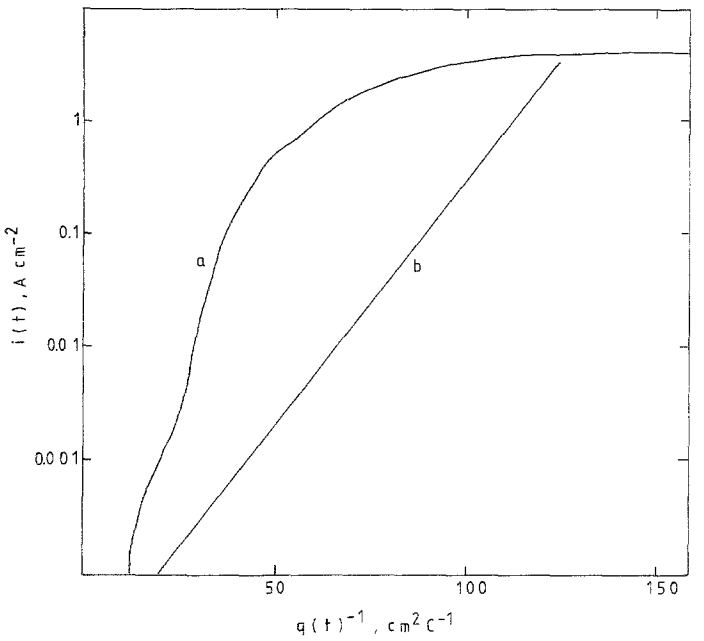

Fig. 6. Decay of scratch current density with charge density passed for indium repassivating in 1.0 M KOH at $E = +345$ mV (versus SHE). (a) Experimental data, $q(t)$; (b) theoretical data for barrier film growth only, $q_f(t)$, calculated from the mean value of $\bar{A}$ (Table 1) and the extrapolated gradient (Fig. 5).

growth according to Equations 6 and 7 still to be occurring and controlling the rate of reaction. Some of this film may, however, from its outermost surface be converted into non-barrier film which does not restrict current flow significantly. This might, for example, be a porous layer overlying the barrier film. Although no charge evolution is involved in the conversion process, the relationship given by Equation 5 and its insertion into Equation 4 are not longer valid. We obtain the *true* barrier film growth charge by extrapolating the lower potentials of Fig. 5 to higher values (denoted by the broken line) to produce $\partial \log i(t)/\partial q(t)^{-1}$, and we use the mean value of $\log \bar{A}$ from Table 1. This provides the pure barrier film growth line shown in Fig. 6. Fig. 6 also shows the observed current decay plot. The difference between the values of $q_0(t)$ (the observed charge density) and $q_f(t)$ (the charge density at any instant associated with the barrier film only, see Fig. 6) is

$$\Delta q(t) = q_0(t) - q_f(t) \qquad (10)$$

and this represents the effective charge associated with the non-barrier film. A plot of $\Delta q(t)/q_f(t)$ against $q_f(t)$ is shown in Fig. 7. Within the scatter each graph shows that the value of $\Delta q(t)/q_f(t)$ is constant, giving $\Delta q(t)/q_f(t) = 0.86$ and 1.2 at $E = +245$ and $+345$ mV (versus SHE), respectively. This means that the fraction of the total film which has been converted into non-barrier film is itself independent of the film thickness and, for both of the transients shown in Fig. 7, represents about one-half of the total film thickness throughout the documented range of charge.

The reasons for the formation of this duplex type of film for $E > +145$ mV (versus SHE) are not yet known. A few features should, however, be pointed out. The excess anodic charge density evolved and ascribed to non-barrier film formation is already documented from fairly early stages of film growth; it is evolved continuously thereafter. Comparison between the two lines given in Fig. 6 shows that excess charge is produced when the charge forming the barrier film is as low as 8–10 mC cm^{-2}. At this film charge, using the parameters given above, the electric field is still very high, with $BV/x(t) \simeq 10$. Although the electric field relaxes continuously as the film grows, the process cannot be defined by onset of low field film growth kinetics, or indeed to a specific value of the field. Neither can it be ascribed to a specific film thickness since anodic charge densities of 8–10 mC cm^{-2} are also observed in film growth kinetics at lower potentials, as shown in Fig. 4. It must therefore be the specific value of the overpotential itself

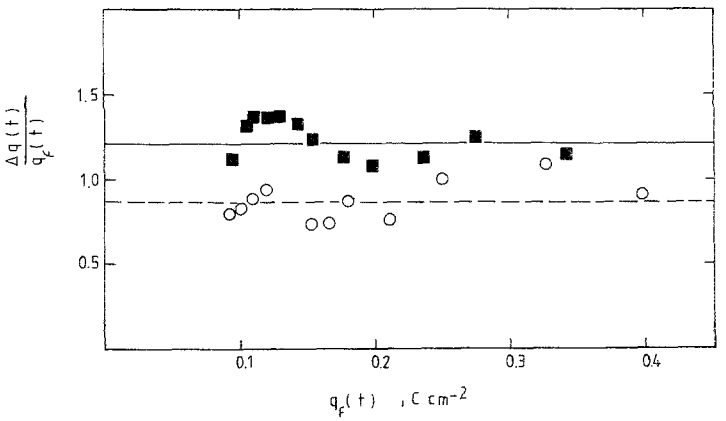

Fig. 7. The ratio of the excess charge density, $\Delta q(t)$, to the barrier film charge density, $q_f(t)$, as a function of $q_f(t)$. ○, $E = +245$ mV (versus SHE); ■, $E = +345$ mV (versus SHE).

which defines the process, despite the fact that indium cannot be further oxidized. It should also be noted that increasing the potential on an indium electrode from +145 to +245 mV (versus SHE) provides a reduction in the steady-state current density (see Fig. 2), albeit a small reduction. This is consistent with the presence of a thicker film on the steady state surface; it is not consistent with a dissolution component or an oxygen evolution component to the anodic charge density.

5. Conclusions

1. The repassivation of indium at pH 14 follows the classic equations of ion conduction through existing film under high electric field. The associated parameters are $\log \bar{A}\,(\mathrm{A\,cm^{-2}}) = -4.94 \pm 0.31$ and $B = (4.8 \pm 0.3) \times 10^{-6}\,\mathrm{cm\,V^{-1}}$.

2. The bare surface mixed potential and the steady-state mixed potential in deaerated aqueous solution of pH 14 are the same. They are also consistent with E_g and with E_0 (between indium and In_2O_3 at pH 14). There is thus no evidence for anodic reactivity at an underpotential. High field film growth occurs at all potentials more positive than E_0.

3. At potentials greater than +145 mV (versus SHE) an excess anodic charge is found over and above that required to satisfy Equation 6. This excess charge is due to growth of a non-barrier film on top of the barrier film. It occupies some 50% of the total anodic film charge, a fraction which is itself approximately independent of the film thickness.

Acknowledgements

We are grateful to Alcan International, Banbury, and to the SERC for the financial support of SJD. Provision of laboratory facilities by Professors R. W. K. Honeycombe and D. Hull is gratefully acknowledged.

References

[1] R. Glicksman and C. K. Morehouse, *J. Electrochem. Soc.* **104** (1957) 589.
[2] T. L. Boswell, *ibid.* **105** (1958) 289.
[3] M. Pourbaix, 'Atlas of Electrochemical Equilibria in Aqueous Solutions', Pergamon Press, Oxford (1966) p. 436.
[4] M. Fleischmann and H. R. Thirsk, *Electrochim. Acta* **6** (1964) 757.
[5] R. D. Armstrong, A. B. Suttie and H. R. Thirsk, *ibid.* **13** (1968) 1.
[6] T. M. Salem and A. A. Ismail, *J. Chem. Soc. (A)* (1970) 2415.
[7] R. Piercy, P. D. Stokes and N. A. Hampson, *Brit. Corros. J.* **8** (1973) 275.
[8] R. Piercy and N. A. Hampson, *J. Appl. Electrochem.* **5** (1975) 1.
[9] G. T. Burstein and R. D. K. Misra, *Electrochim. Acta* **28** (1983) 363.
[10] G. T. Burstein and P. I. Marshall, *Corros. Sci.* **23** (1983) 125.
[11] G. T. Burstein and G. W. Ashley, *Corrosion* **40** (1984) 110.
[12] S. J. Duncan and G. T. Burstein, presented at 'Control and Exploitation of the Corrosion of Aluminium Alloys', Cranfield (1983).
[13] G. T. Burstein and R. D. K. Misra, submitted to *J. Appl. Electrochem.*
[14] N. Cabrera and N. J. Mott, *Rep. Prog. Phys.* **12** (1948) 163.
[15] R. C. Weast (ed), 'Handbook of Chemistry and Physics', 64th edn, CRC Press, Cleveland (1983) p. B-118.
[16] P. I. Marshall and G. T. Burstein, *Corros. Sci.* **24**

(1984) 462.
[17] T. P. Hoar, in 'Modern Aspects of Electrochemistry', Vol. 2 (edited by J. O. M. Bockris), Butterworths, London (1959) p. 262.
[18] Powder Diffraction Data, Joint Committee on Powder Diffraction Standards, National Bureau of Standards, Washington, pp. 6–416.
[19] G. T. Burstein and R. D. K. Misra, *Electrochim. Acta* **28** (1983) 371.
[20] G. T. Burstein and G. W. Ashley, *Corrosion* **39** (1983) 241.